Available online at www.sciencedirect.com
SCIENCE DIRECT®
Optics Communications 215 (2003) 333–343
OPTICS COMMUNICATIONS
www.elsevier.com/locate/optcom

Electro-optical properties of $Sn_2P_2S_6$

D. Haertle[a,*], G. Caimi[a], A. Haldi[a], G. Montemezzani[a], P. Günter[a], A.A. Grabar[b], I.M. Stoika[b], Yu.M. Vysochanskii[b]

[a] *Nonlinear Optics Laboratory, Institute of Quantum Electronics, ETH Hönggerberg HPF E18, Swiss Federal Institute of Technology, CH-8093 Zürich, Switzerland*
[b] *Institute of Solid State Physics and Chemistry, Uzhgorod National University, 88 000 Uzhgorod, Ukraine*

Received 30 August 2002; received in revised form 31 October 2002; accepted 28 November 2002

Abstract

The electro-optical (EO) properties of monoclinic $Sn_2P_2S_6$ single crystals are measured by direct interferometric technique for electric fields applied parallel to the crystallographic x-axis that lies near the spontaneous polarization vector. The room temperature free EO coefficient r^T_{111} reaches 174 ± 10 pm/V at $\lambda = 633$ nm and shows only weak dispersion in the wavelength range between $\lambda \approx 0.6, \ldots, 1.3$ μm. Corresponding values of r^T_{221} and r^T_{331} at $\lambda = 633$ nm are 92 ± 8 and 140 ± 18 pm/V, respectively. The temperature dependence of the EO coefficients near the structural phase transition at $T_C = 65$ °C is well described by a Curie–Weiss law with a peak value $r^T_{111} \cong 4500$ pm/V. The ratio between the free and clamped EO coefficients is determined at the wavelength $\lambda = 633$ nm by applying a fast pulsed electric field instead of an AC field and measuring the temporal evolution of the electrically induced refractive index change. The values are $r^S_{111}/r^T_{111} = 0.30 \pm 0.02$, $r^S_{221}/r^T_{221} = 0.12 \pm 0.02$ and $r^S_{331}/r^T_{331} = 0.30 \pm 0.09$.

PACS: 78.20.Jq; 78.20.Ci; 77.80.Bh; 42.70.Mp

Keywords: $Sn_2P_2S_6$; Electro-optics; Polarization-optical coefficients; Refractive index

1. Introduction

Tin thiohypodiphosphate ($Sn_2P_2S_6$) is a wide band gap semiconductor ferroelectric with interesting nonlinear optical properties [1] and wide optical transparency range extending from $\lambda = 0.53$ μm to $\lambda = 8$ μm [2]. In addition it is also photorefractive with fast photorefractive grating recording times and large refractive index change in the red and near infrared spectral region [3,4], opening interesting possibilities for applications in connection with laser diode sources.

For electro-optics or photorefractive applications the knowledge of the electro-optical (EO) properties is of fundamental importance. Unfortunately, to date individual components of the EO tensor of $Sn_2P_2S_6$ are still unknown. Presently available data on EO properties are restricted to estimations based on the spontaneous EO effect

* Corresponding author. Tel.: +41-1-633-23-38; fax: +41-1-633-10-56.
E-mail address: haertle@iqe.phys.ethz.ch (D. Haertle).

0030-4018/02/$ - see front matter
PII: S0030-4018(02)02251-4

induced by the spontaneous polarization [5], to measurements of the field-induced birefringence giving values for some mixed coefficients [6] and to effective values indirectly estimated from photorefractive beam-coupling experiments [3,4,7–9].

In the present work we report on the direct determination of the most important EO tensor components of $Sn_2P_2S_6$, i.e. those for applied electric fields oriented parallel to the crystallographic x-axis, that is nearly parallel to the spontaneous polarization. A standard interferometric set-up with AC applied fields was used [10–12]. Measurements are performed in the wavelength range between 594 and 1313 nm at room temperature as well as in the temperature range between room temperature and the phase transition for $\lambda = 633$ nm. Finally, the ratios of clamped to free EO coefficients were determined by applying fast rising electric pulses to the crystal using the method described earlier in [13]. The large values of the EO coefficients determined here (up to 174 pm/V at room temperature and 4510 pm/V near the phase transition temperature of 65 °C for $\lambda = 633$ nm) and its weak dispersion towards the infrared confirm that this material seems attractive for EO or photorefractive applications at red and infrared wavelengths.

2. Crystallographic and optical properties

$Sn_2P_2S_6$ is a proper ferroelectric with monoclinic point group symmetry m at room temperature. The crystal undergoes a second-order phase transition to the centrosymmetric paraelectric phase (point group $2/m$) at the temperature $T_C = 338$ K [14]. For the unit cell chosen by Dittmar and Schafer [15] which we refer to in this work, the lattice parameters are $a = 0.9378$ nm, $b = 0.7448$ nm, $c = 0.6513$ nm, and $\beta = 91.15°$. We choose the right-handed coordinate system which is shown in Fig. 1 together with the crystallographic axes. The x-axis is defined parallel to the [1 0 0] crystallographic direction (a-axis), that is 13° off the spontaneous polarization vector $\mathbf{P}_S$ [16,17], while the y-axis is normal to the symmetry plane and corresponds to the crystallographic b-axis. Finally, the z-axis is chosen perpendicular to

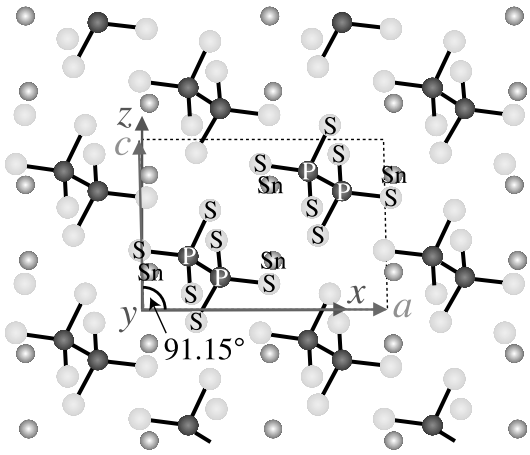

Fig. 1. Structure of $Sn_2P_2S_6$. The symmetry plane is parallel to the plane of the figure. The unit cell is indicated by the dashed lines.

x and y and deviates from the [0 0 1] direction by 1.15°. In accordance to the IEEE standard on piezoelectric materials [18], the positive direction of the x-axis and the z-axis is set so that the piezoelectric constants d_{111} and d_{333} are positive and $+y$ is chosen so that xyz is a right-handed system. In this system $\mathbf{P}_S \cdot \hat{\mathbf{x}} > 0$ and $\mathbf{P}_S \cdot \hat{\mathbf{z}} > 0$, where $\hat{\mathbf{x}}$ and $\hat{\mathbf{z}}$ are the unit vectors in x and z-direction. Note that the coordinate system used here corresponds to the one used in most of the previous investigations of EO, nonlinear optical and photorefractive properties. Alternative choices for the coordinate system may be related to the main axes of the low-frequency dielectric tensor or of the optical indicatrix, the latter choice was used for instance in [5]. We prefer the use of the coordinate system described above because the crystallographic axes do not suffer from the variations in the orientation of the dielectric tensor and of the optical indicatrix observed by varying temperature, frequency of the electric field, or light wavelength [5] (see Fig. 2).

The linear optical properties of SPS were first reported in [5], where the main values of the refractive indices, the indicatrix orientation and its variation with temperature were measured. The main values of refractive indices at 633 nm and room temperature are $n_1 = 3.038, n_2 = 2.928$ and $n_3 = 3.133$. On the basis of the available data on

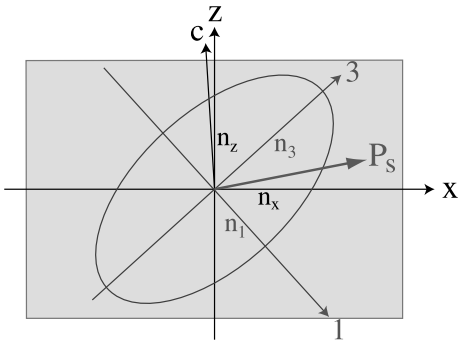

Fig. 2. Position of spontaneous polarization and indicatrix in the *xz*-plane at room temperature.

the temperature variations of the refractive indices, dielectric constant and spontaneous polarization $\mathbf{P}_S$, the "spontaneous" linear EO coefficients in the ferroelectric phase as well as the quadratic (Kerr) polarization-optical constants in the paraelectric phase have been evaluated [5].

Sellmeier coefficients were determined from available refractive index data [19] (Fig. 3) by fitting a Sellmeier equation of the form

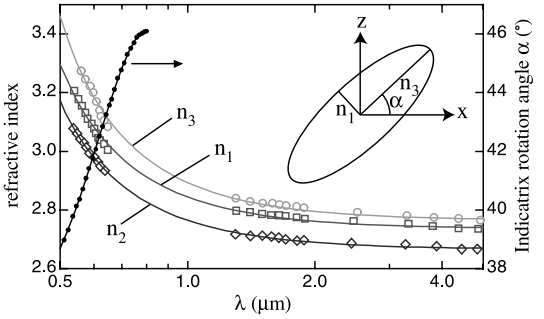

Fig. 3. Refractive indices (left-hand scale) and rotation angle of the indicatrix in the *xz* plane (right-hand scale). The measurements [5,19] are fitted with a single oscillator Sellmeier model whose parameters are given in Table 1.

$$n^2(\lambda) - 1 = \frac{S_0\lambda_0^2}{1-(\lambda_0/\lambda)^2}, \tag{1}$$

where S_0 and λ_0 are the oscillator strength and wavelength of a single-oscillator Sellmeier model, and $E_0 = (hc/\lambda_0)$ is the oscillator energy. The Sellmeier coefficients for the main axes of the index ellipsoid are given in Table 1.

Note that $Sn_2P_2S_6$ obeys well the empirical law of Wemple and DiDomenico [20,21] that the ratio $E_0/S_0 = (6 \pm 0.5) \times 10^{-14}$ eV m^2 for most inorganic crystals.

The main axes of the indicatrix corresponding to the refractive indices n_1 and n_3 are rotated by about 45° around the *b*-axis with respect to the crystallographic axes. Therefore the refractive indices along the crystallographic axes *x* and *y* are

$$n_x = \left(\frac{\sin^2\alpha}{n_1^2} + \frac{\cos^2\alpha}{n_3^2}\right)^{-\frac{1}{2}} \quad \text{and} \quad n_y = n_2,$$

where α is the angle between the axis *x* and axis 3 (largest refractive index). For $\lambda = 633$ nm and $T = 295$ K one has $\alpha \approx 43°$ and $n_x = 3.088$.

3. Electro-optical effect

The third-rank EO tensor for materials of monoclinic point group *m* contains 10 independent components. In our coordinate system $(x, y, z) = (1, 2, 3)$ it has the form

$$r_{ijk} = \begin{pmatrix} r_{111} & 0 & r_{113} \\ r_{221} & 0 & r_{223} \\ r_{331} & 0 & r_{333} \\ 0 & r_{322} & 0 \\ r_{131} & 0 & r_{133} \\ 0 & r_{122} & 0 \end{pmatrix} \tag{2}$$

with the inherent symmetry ($r_{ijk} = r_{jik}$). The inverse dielectric tensor at optical frequency is

Table 1
Sellmeier coefficients for dispersion of the refractive index of $Sn_2P_2S_6$ at room temperature

	S_0 (μm^{-2})	λ_0 (nm)	E_0 (eV)	E_0/S_0 (10^{-14} eV m^2)
n_1	76 ± 4	292 ± 7	4.24 ± 0.10	5.6 ± 0.3
n_2	75 ± 5	284 ± 5	4.37 ± 0.08	5.8 ± 0.4
n_3	68 ± 3	313 ± 6	3.96 ± 0.08	5.8 ± 0.3

$$\left(\frac{1}{n^2}\right)_{ij} = \begin{pmatrix} \frac{1}{n_{11}^2} & & \frac{1}{n_{13}^2} \\ & \frac{1}{n_{22}^2} & \\ \frac{1}{n_{13}^2} & & \frac{1}{n_{33}^2} \end{pmatrix} \tag{3}$$

with the outer-diagonal terms $\frac{1}{n_{13}^2}$ being responsible for the rotation of the main axes of the indicatrix with respect to the crystallographic axes. After applying an electric field $\mathbf{E} = (E, 0, 0)$ along the x-axis the change of this tensor is expressed as

$$\Delta\left(\frac{1}{n^2}\right)_{ij} = r_{ijk}E_k = \begin{pmatrix} r_{111}E & 0 & r_{131}E \\ 0 & r_{221}E & 0 \\ r_{131}E & 0 & r_{331}E \end{pmatrix}, \tag{4}$$

where Einstein's summation convention over equal indices is used. In the measurements described below we have used only input light polarizations that correspond to an eigenpolarization in the sample, leading only to a phase modulation of the signal beam. The corresponding change of the main axes of the indicatrix is then

$$\Delta\left(\frac{1}{n^2}\right) = \Delta\left(\frac{1}{n^2}\right)_{ij} \hat{d}_i \hat{d}_j.$$

Here $\hat{\mathbf{d}}$ is the unit vector along the polarization direction. By choosing appropriate geometries individual elements or linear combinations of the four independent EO coefficients r_{111}, r_{221}, r_{331}, r_{131} can be determined.

4. Samples

Optical quality $Sn_2P_2S_6$ single crystals were produced by the conventional vapor–transport technique [14,22] using iodine as a transporter. We used nominally pure samples exhibiting low photorefractive effects. Samples with dimensions $5.21 \times 7.58 \times 5.83$ mm^3, $5.44 \times 5.72 \times 2.79$ mm^3 and $5.07 \times 5.38 \times 4.85$ mm^3 along x, y and z axes, respectively, were polished, and electrically poled by heating above T_C and slowly cooling them down to room temperature under an electric field of about 1 kV/cm applied along the x-direction. Gold evaporated electrodes were used for poling and for inducing the refractive index changes by the electric field. The single domain state was controlled using light scattering by domain walls in $Sn_2P_2S_6$ described in [23]. This method permits an easy visualization of polydomain areas within the sample.

5. Experiments

5.1. Unclamped EO coefficients

In our study the linear EO coefficients were measured using a standard Michelson interferometer [10–12]. This method allows the determination of the individual components of the EO tensor including their sign. The experimental set-up was similar to the one used in [10,11] and is shown in Fig. 4. The typical value for the applied electric field amplitude was $E \cong 3$ V/cm. For the investigation of the wavelength dependence of the tensor components r_{111} and r_{221} the measurements were carried out at six different light wavelengths: 594 and 633 nm (He–Ne laser), 817 and 877 nm (Ti:Sapphire laser), 1064 nm (Nd:YAG laser) and 1313 nm (Nd:YLF laser). The studied $Sn_2P_2S_6$ samples were mounted free in one arm of the interferometer, and the light intensity in the output interference picture was measured by a photodetector. When an electric field $\mathbf{E} = (E, 0, 0)$ is applied to the sample the induced phase shift between the interfering beams is

$$\Delta\phi = \frac{2\pi}{\lambda} L\Delta n + \frac{2\pi}{\lambda}(n-1)\Delta L, \tag{5}$$

$$= -\frac{\pi}{\lambda} L n^3 r_{\text{eff}} E + \frac{2\pi}{\lambda} L(n-1) d_{\text{eff}} E, \tag{6}$$

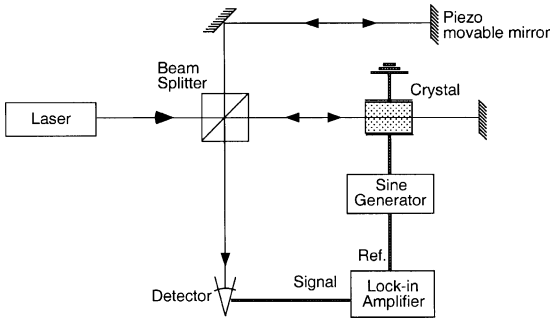

Fig. 4. Interferometric set-up for measuring the unclamped EO coefficients r_{ijk}^T, using a low frequency sine modulation.

where L is the length of the path in the crystal (twice the length of the crystal), n is the refractive index seen by the eigenwave, r_{eff} is the effective EO coefficient, which is either equal to one of the coefficients appearing in (4) or to a linear combination of them and d_{eff} is the effective piezoelectric coefficient. The second term on the right-hand-side of (6) is due to the piezoelectric length change of the crystal and was evaluated using the known piezoelectric constants of the crystal [16]. This piezoelectric effect represents a relatively small correction to the EO coefficients measured (about 3% for r_{111}, 8% for r_{221} and 10% for r_{331}).

If the applied field is a weak modulated sine-wave signal with frequency Ω ($V = E \cdot d \ll V_\pi$, where $V_\pi = \lambda/(Ln^3 r_{\text{eff}})$), the measured intensity at the interferometer output is of the form

$$I = I_1 + I_2 - 2\sqrt{I_1 I_2}\frac{2\pi}{\lambda}L \times (n^3 r_{\text{eff}} - 2(n-1)d_{\text{eff}})E\sin(2\pi\Omega t), \quad (7)$$

where I_1 and I_2 are the intensities of the beams in the two arms of the interferometer. In our measurements the working point was adjusted by means of the external piezoelectrically movable mirror in Fig. 4 and the amplitude of the modulated signal in (7) was determined using a lock-in amplifier. Finally the value of the effective EO coefficients r_{eff} were determined by using (6) and (7). Note that for the measurements of the temperature dependence the set-up in Fig. 4 was slightly modified by placing the $Sn_2P_2S_6$ crystal inside an oven allowing to change the sample temperature above the phase transition at 65 °C.

At low frequencies of the applied field ($\Omega < 500$ Hz) we found that significant photoconductive screening of the applied field occurs already for intensities of the optical beam in the order of 100 $\mu W/cm^2$ ($\lambda = 633$ nm). This would lead to reduced values of the measured EO coefficient. This effect disappears if the electric field frequency is increased to $\Omega \approx 1$ kHz. Therefore all the measurements were performed at the low intensity described above and at $\Omega \approx 1$ kHz. For the measurements of the EO coefficients r_{ij1} the electric field has to be applied parallel to the x-axis, which is close to the spontaneous polarization. Since the dielectric constant is maximal parallel to the spontaneous polarization, we expect the largest EO tensor elements in this configuration.

The coefficients r_{111} and r_{221} were measured with a beam propagation vector along z-axis and polarization along the x-axis and the y-axis, respectively. The other two coefficients r_{331} and r_{131} were calculated from two measurements with beam propagation along the y-axis and polarizations α and $\alpha + \frac{\pi}{2}$ off the x-axis, the two eigenpolarizations in this geometry. From the measurement of r_α, $r_{\alpha+\frac{\pi}{2}}$ we obtain

$$r_{331} = r_\alpha + r_{\alpha+\frac{\pi}{2}} - r_{111}, \quad (8)$$

$$r_{131} = \frac{r_\alpha \cos^2\alpha - r_{\alpha+\frac{\pi}{2}}\sin^2\alpha - r_{111}\cos 2\alpha}{\sin 2\alpha} \quad (9)$$

by rotating the coordinate system by an angle α about the y-axis, where r_α and $r_{\alpha+\frac{\pi}{2}}$ are the measured effective coefficients. Since r_{331} and r_{131} are obtained by summing and subtracting the results of different measurements, the relative errors of their values are larger than those of r_{111} and r_{221}.

The values of the measured EO coefficients at $\lambda = 633$ nm and room temperature are given in Table 2. The values are the average of measurements on two crystals (three crystals for r^T_{111} and r^T_{221}) and three different positions per crystal. The dispersion of the values from different positions and crystals is generally within the experimental error given in Table 2. This table shows that $Sn_2P_2S_6$ possesses very large EO coefficients r_{111}

Table 2
Electro-optical coefficients of $Sn_2P_2S_6$ at $\lambda = 633$ nm and room temperature

	Property	Value
Unclamped EO coefficients (pm/V)	r^T_{111}	$+174 \pm 10$
	r^T_{221}	$+92 \pm 8$
	r^T_{331}	$+140 \pm 18$
	r^T_{131}	-25 ± 15
Clamped EO coefficients (pm/V)	r^S_{111}	$+50 \pm 5$
	r^S_{221}	$+11 \pm 3$
	r^S_{331}	$+42 \pm 10$
	r^S_{131}	-11 ± 8
Ratio r^S/r^T	r^S_{111}/r^T_{111}	0.30 ± 0.02
	r^S_{221}/r^T_{221}	0.12 ± 0.02
	r^S_{331}/r^T_{331}	0.30 ± 0.09

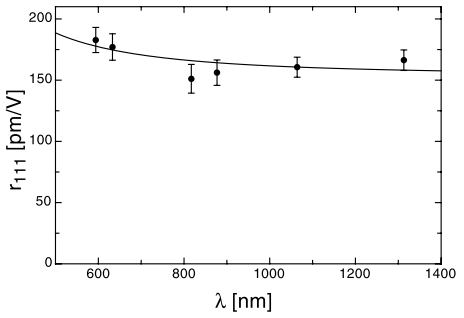

Fig. 5. Dispersion of r_{111}^T at room temperature. The theoretical curve is given by Eq. (10) and the parameters reported in the text.

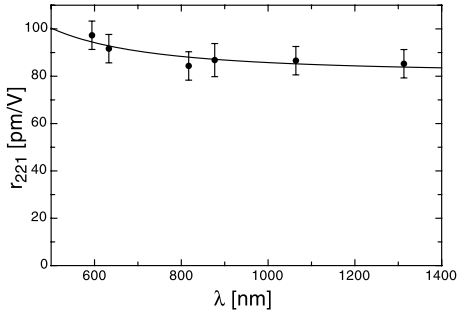

Fig. 6. Dispersion of r_{221}^T at room temperature. The theoretical curve is given by Eq. (10) and the parameters reported in the text.

and r_{331}, confirming the suitability of this crystal for EO and photorefractive applications. The reduced half-wave voltage $V_\pi = \lambda/(n^3 r)$ of $Sn_2P_2S_6$ is very low compared to other materials, since both n and r are large. For $\lambda = 633$ nm and r_{111}^T the reduced half-wave voltage is $V_\pi = 124$ V. As a comparison, for the standard material $LiNbO_3$ is $V_\pi = \lambda/(n_e^3 r_{333}) = 1885$ V.

The wavelength dependence of r_{111} and r_{221} at room temperature is shown in Figs. 5 and 6. The experimental values are compared with the results of a one oscillator model which uses polarization potentials dE_0/dP (change of the oscillator energy $E_0 = hc/\lambda_0$ with crystal polarization) and dispersion constants

$$K = -\frac{\frac{\partial(S_0\lambda_0)}{\partial P}}{S_0\frac{\partial\lambda_0}{\partial P}}$$

as parameters [20,21],

$$r = \epsilon_0(\epsilon - 1)\left(1 - \frac{1}{n^2}\right)^2 \times \frac{\frac{dE_0}{dP}}{S_0 hc\lambda_0}\left((1-K) + (1+K)\frac{\lambda_0^2}{\lambda^2}\right). \quad (10)$$

In (10) ϵ_0 is the dielectric permittivity of vacuum, S_0 and λ_0 are the oscillator strength and wavelength of a single-oscillator Sellmeier model (given in Table 1), and K describes the change of the interband oscillator strength induced by polarization changes. Eq. (10) is derived from the so called polarization potential model, which assumes a "sensible" parametrization of the linear susceptibility followed by differentiation with respect to the applied crystal polarization.

As can be seen in Figs. 5 and 6 the dispersion of r_{111} and r_{221} is small, with EO coefficients at $\lambda = 1313$ nm nearly as large as in the red. Note however, that the absorption is smaller in the infrared region, which would benefit EO devices operating at these wavelengths. With $\epsilon_{11} = 230$ [4] we can determine $dE_0/dP = (2.8 \pm 0.6) \times 10^{-19}$ V m^2 and $K = -0.5 \pm 0.4$ for r_{111}, while for r_{221} they are $dE_0/dP = (1.6 \pm 0.4) \times 10^{-19}$ V m^2 and $K = -0.4 \pm 0.4$.

The temperature dependence of r_{111} and r_{221} for $T < T_C$ is shown in Figs. 7 and 8. As expected, the EO coefficients grow according to mean field the-

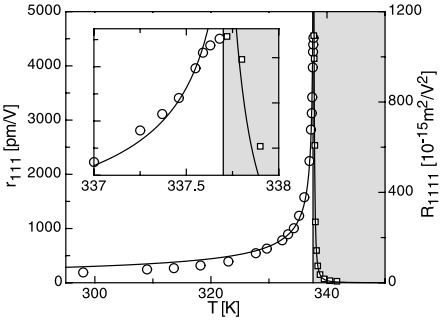

Fig. 7. Temperature dependence of r_{111}^T ($T < T_C$) and R_{1111}^T ($T > T_C$, grey region) at $\lambda = 633$ nm. The theoretical line is according to (11) and (14) with the parameters $T_C = 64.7$ °C and $AC\epsilon_0 g = 1863\ \sqrt{°C}$ pm/V for the ferroelectric phase, and $T_C = 64.4$ °C and $\epsilon_0^2 D^2 g = 57.2 \times 10^{-15}$ °C^2 m^2/V^2 for the paraelectric phase. The inset shows the same data near the phase transition temperature, in the same y-scale.

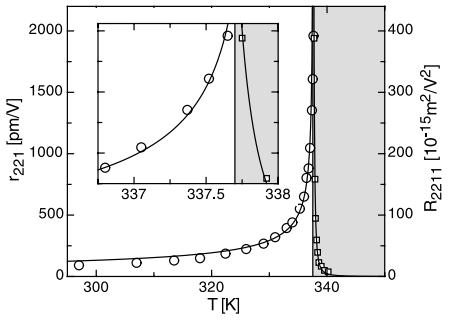

Fig. 8. Temperature dependence of r^T_{221} ($T < T_C$) and R^T_{2211} ($T > T_C$, grey region) at $\lambda = 633$ nm. The line is a fit according to (11) and (14) with the fitted parameters $T_C = 64.8$ °C and $AC\epsilon_0 g = 808.5\ \sqrt{°C}$ pm/V for the ferroelectric phase, and $T_C = 64.3$ °C and $\epsilon_0^2 D^2 g = 28.8 \times 10^{-15}\ °C^2\ m^2/V^2$ for the paraelectric phase. The inset shows the same data near the phase transition temperature, in the same y-scale.

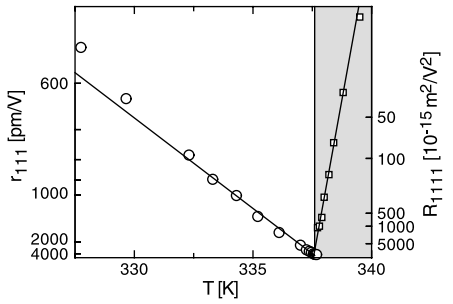

Fig. 9. Same curve as in Fig. 7, but in inverse square scale for r_{111} below T_C and inverse square root scale for R_{1111} above T_C.

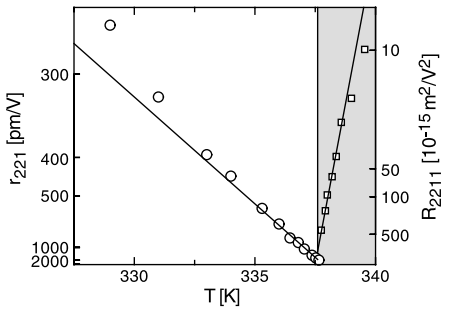

Fig. 10. Same curve as in Fig. 8, but in inverse square scale for r_{221} below T_C and inverse square root scale for R_{2211} above T_C.

ory of second-order phase transitions with a Curie–Weiss law $\epsilon = C/(2(T_C - T))$ and $P_S = A(T_C - T)^{\frac{1}{2}}$. Therefore the EO coefficients are

$$r \simeq 2\epsilon_0(\epsilon - 1)gP_S \simeq AC\epsilon_0 g(T_C - T)^{-\frac{1}{2}}, \tag{11}$$

where C is the Curie constant, A is a material constant that can be fitted from the temperature dependence of P_S and g is a suitable quadratic polarization-optic coefficient. The full line in Figs. 7 and 8 is according to (11). In Figs. 9 and 10 r_{111}^{-2} and r_{221}^{-2} are shown as a function of temperature. In proximity of $T_C (T_C - T \lesssim 10$ °C), r^{-2} depends linearly on $T_C - T$.

Above T_C the crystal is in the paraelectric phase and the linear EO tensor **r** vanishes due to the centrosymmetric structure. The quadratic EO tensor **R** is then the lowest order EO tensor. Superposing a DC electric field $\mathbf{E}_{dc} = (E_{dc}, 0, 0)$ to the sinusoidal signal field allows to measure a first-order effect of **R**:

$$\begin{aligned}\Delta\left(\frac{1}{n^2}\right)_{ij} &= R_{ijkl}E_kE_l \\ &= R_{ij11}(E_{dc} + E_0\sin(\Omega t))^2 \\ &= (R_{ij11}E_{dc})E_{dc} + 2(R_{ij11}E_{dc})E_0\sin(\Omega t) \\ &\quad + (R_{ij11}E_0)E_0\sin^2(\Omega t) + \cdots\end{aligned} \tag{12}$$

The first term in (12) does not depend on the modulation field so that it generates only a static deformation of the indicatrix. The second term describes a change in the indicatrix linear to the applied signal field so that this term is detected in the lock-in at the frequency Ω as an equivalent linear EO tensor

$$r^{\Omega}_{ijk} = 2R_{ijk1}E_{dc}. \tag{13}$$

The third term describes the pure quadratic EO effect. In our measurements at temperatures above T_C the applied bias field was $E_{dc} = 20$ V/cm.

Above the critical point T_C the temperature dependence of the quadratic EO coefficient can be approximately described by the function

$$R \simeq \epsilon_0^2(\epsilon - 1)^2 g \simeq \epsilon_0^2 \frac{D^2}{(T - T_C)^2} g, \tag{14}$$

where D is a modified Curie constant and g is a suitable quadratic polarization-optic coefficient. The constants $\epsilon_0^2 D^2 g$ for R_{1111} and R_{2211} are given in Figs. 7 and 8, respectively. Fig. 9 shows R_{1111} in

inverse square root scale showing the linear relationship of $R^{-1/2}$ versus $(T - T_C)$. The similar curve for R_{2211} is shown in Fig. 10.

5.2. Clamped EO coefficients

Recently we have introduced a new method for determining the ratio r^S/r^T between the clamped and unclamped (free) EO coefficients [13]. This method is based on applying a fast electric field pulse to the crystal instead of an AC field and considering the time dependence of the field-induced refractive index change. This allows to separate the fast (clamped) part r^S of the EO tensor from the slower contribution due to acoustic phonons. The instantaneous intensity change upon applying the voltage pulse (step in Fig. 11) is proportional to r^S, while the stationary value is proportional to r^T. With the acoustic contribution to r^T also a mechanical ringing of the crystal appears, induced by the piezoelectric effect.

The same interferometric set-up as above was used (Fig. 4), but the sine wave generator was replaced by a pulse generator (Tabor 8201) to create square pulses with rise time shorter than 12 ns. The typical pulse voltage amplitude for an approximately cubic crystal of side length ≅0.5 cm was 1 V. The output signal of the interferometer was detected by a fast photodiode attached directly to an oscilloscope and averaged over 140 pulses. For these measurements a larger light intensity of the order of 100 mW/cm^2 had to be used. Even though nominally pure crystals were used, the large photoconductivity of $Sn_2P_2S_6$ crystals at $\lambda = 633$ nm leads to a strong screening of the applied field already before the end of the pulse. Therefore, the unclamped contribution to the signal has to be found by extrapolating the signal curve to the beginning of the pulse. This can be done because the build-up time of the screening is much longer than the response time of the acoustic EO contribution.

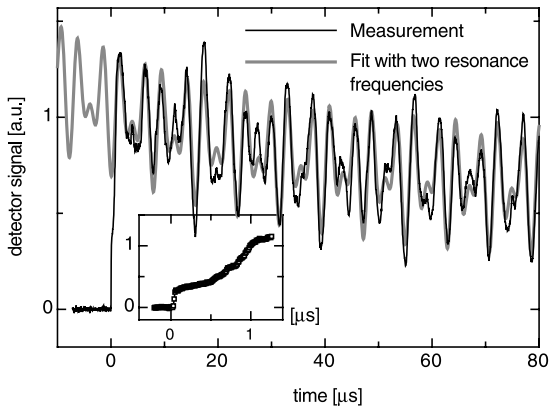

Fig. 11. Measurement of ratio r^S/r^T: a sharp square electric field pulse starts at $t = 0$ s and lasts 10 ms. r^S/r^T is given by the ratio of the height of the step at $t = 0$ s ($\sim r^S$, inset) and the extrapolated signal at $t = 0$ s ($\sim r^T$), which is scaled to unity in this figure. The oscillations are due to resonant mechanical oscillations with frequencies $\nu_1 = 255$ kHz and $\nu_2 = 382$ kHz and the exponential decay of the signal is due to screening of the electric field in the illuminated region.

The oscillations in Fig. 11 are given by resonant mechanical modes of the crystal and are fitted with $\nu_1 = 255$ kHz and $\nu_2 = 382$ kHz. The same crystal was analyzed using an impedance spectrometer, which permits to roughly calculate its dielectric function through its capacitance. Among the many resonances of $\epsilon_{11}(\omega)$, resonances at ν_1 and ν_2 were clearly visible.

The measured ratios r^S/r^T and the clamped EO coefficients r^S are shown in Table 2. The dominant part of r^T is given by the contribution from acoustic phonons, a combination of the piezoelectric and the elasto-optic effect, and the anisotropy in the y-direction is more pronounced for the EO coefficient r^S than for the acoustic contribution to r.

6. Discussion

Direct measurement of the EO effect was reported earlier by Kroupa et al. in [6] by measuring the birefringence for the longitudinal geometry, where both the light beam propagation and the applied electric field are directed along the x-direction. Only an effective value of the EO coefficient of the type $r_a = r_{331} - (n_2/n_z)^3 r_{221}$ can be obtained in this geometry, with n_z being the refractive index for light polarization parallel to the z-axis. We obtain the value $r_a = 62 \pm 20$ pm/V based on Table 2. This is slightly higher than the approximated value of 51 pm/V that can be ex-

trapolated to room temperature from the data in [6].

In order to get an additional confirmation for our data, we also performed experiments using the same type of setup as in [6], but with the light propagating along the z-direction and field along the x-direction. The effective coefficient in this configuration is $r_c = r_{111} - (n_2/n_x)^3 r_{221} = 100 \pm 5$ pm/V. This agrees well with the value $r_c = 96 \pm 13$ pm/V calculated from the EO coefficients r_{111} and r_{221} measured interferometrically (Table 2).

The EO coefficients measured in this work are also higher than the ones estimated by using light diffraction from photorefractive gratings, $r_{111}^{\mathrm{PR}} \cong 130$ pm/V at $\lambda = 900$ nm [8] and $r_{111}^{\mathrm{PR}} \cong 37 - 53$ pm/V at $\lambda = 1064$ nm [3]. This is expected due to the partial clamping of the piezo-elasto-optical contributions to the EO effect that occur with a spatially modulated field [24] and possible electron-hole competition [25,26] or other effects reducing the apparent EO coefficient in photorefractive measurements [27].

Note also, that the ratio $r_{221}^T/r_{111}^T = 0.54 \pm 0.04$ pm/V at $\lambda = 1064$ nm is higher than $r_{221}^{\mathrm{PR}}/r_{111}^{\mathrm{PR}} = 0.38 \pm 0.02$ [7] measured by Hellwig et al. at the same wavelength, while $r_{221}^T/r_{331}^T = 0.66 \pm 0.10$ pm/V at $\lambda = 633$ nm compares well to $r_{221}^{\mathrm{PR}}/r_{331}^{\mathrm{PR}} \cong 0.59$ at $\lambda = 1064$ nm [9]. Also here the discrepancy between our ratios and those obtained by photorefractive investigations might be attributed to the same reasons.

The polarization-optic coefficients f_{ijm} that relate the change of the optical indicatrix with the crystal polarization $\mathbf{P}$ as $\Delta(1/n^2)_{ij} = f_{ijm}P_m$ are often regarded as more fundamental constants since they show much smaller variations from material to material than the EO coefficients. The EO coefficients r_{ijk} are related to f_{ijm} by the expression $r_{ijk} = \epsilon_0 f_{ijm}(\epsilon_{mk} - \delta_{mk})$, where δ_{mk} is the Kronecker's delta. For the elements r_{ij1} in point group m this expression reduces to

$$r_{ij1} = \epsilon_0 f_{ij1}(\epsilon_{11} - 1) + \epsilon_0 f_{ij3}\epsilon_{13} \tag{15}$$

for $ij = 11, 22, 33$ and $13 = 31$. The dielectric tensor in $Sn_2P_2S_6$ is rotated by only about 13° with respect to the crystallographic x-axis and the ratio between ϵ_{11}, which is the largest element of the dielectric tensor, and the outer diagonal element ϵ_{13} is $\epsilon_{11}/\epsilon_{13} \cong 6$. It is therefore reasonable to assume that the main contribution to the elements r_{ij1} in Eq. (15) comes from the first term on the right-hand side. By neglecting the second term one obtains a rough estimation for the polarization-optic coefficients of the form $f_{ij1} \approx r_{ij1}/(\epsilon_0\epsilon_{11})$. Using $\epsilon_{11} \cong 230$ and the values shown in Table 2 one obtains $f_{111} \cong 0.089$ m^2/C, $f_{221} \cong 0.046$ m^2/C, $f_{331} \cong 0.072$ m^2/C and $f_{131} = f_{311} \cong 0.012$ m^2/C. These values are of the same order of magnitude as the polarization-optical coefficients observed in several inorganic oxide crystals such as $KNbO_3$ or $BaTiO_3$ [28]. This indicates that the main reason for the observed high EO coefficients of $Sn_2P_2S_6$ is the large dielectric constant.

It is possible to estimate the quadratic polarization-optic coefficients g_{ijkl} of the upper paraelectric phase from the EO coefficients r_{ijk}. From crystal optic measurements Grabar et al. [5] determined four elements of the quadratic polarization-optic tensor in the coordinate system corresponding to the main axes of the indicatrix. By transforming their values to the coordinate system used in this work one obtains [1]

$$\begin{aligned} &g_{1111} \cong 0.256 \text{ m}^4/\text{C}^2, \\ &g_{2211} \cong 0.13 \text{ m}^4/\text{C}^2, \\ &g_{3311} \cong 0.154 \text{ m}^4/\text{C}^2, \\ &g_{1311} \cong -0.035 \text{ m}^4/\text{C}^2. \end{aligned} \tag{16}$$

It has been generally assumed [20,21] that the quadratic polarization-optic coefficients g_{ijkl} do not depend on temperature (at least not in first approximation). Therefore in ferroelectric materials the linear EO effect is regarded as the same quadratic effect of the centrosymmetric high temperature phase biased by the spontaneous polarization $\mathbf{P}_S$. That is

$$\Delta\left(\frac{1}{n^2}\right)_{ij} = g_{ijkl}P_kP_l \tag{17}$$

[1] Note that the left-hand scale of [5, Fig. 2] has to be reduced by a factor 10, consequently the last equation of page 2088 in [5] should read $(M_{51} + M_{53} + M_{55})/2 = 5.01 \times 10^{-2}$ m^4/C^2 in that reference.

with polarization $\mathbf{P} = \mathbf{P}_S + \mathbf{P}_{ind}$ and $\mathbf{P}_{ind} = \epsilon_0(\epsilon - \delta)\mathbf{E}$. In $Sn_2P_2S_6$ one has $\mathbf{P}_S = (P_S \cos\gamma, 0, P_S \sin\gamma)$ with $P_S \cong 14\ \mu C/cm^2$ and $\gamma \cong 13°$ at room temperature. Combining (4) with (17) one gets

$$r_{ijk} = 2\epsilon_0(\epsilon_{mk} - \delta_{mk})g_{ijml}P_S l. \tag{18}$$

It follows that

$$\begin{aligned} r_{ij1} =& 2\epsilon_0(\epsilon_{11} - 1)g_{ij11}P_S \cos\gamma + 2\epsilon_0\epsilon_{31}g_{ij13}P_S \cos\gamma \\ &+ 2\epsilon_0(\epsilon_{11} - 1)g_{ji13}P_S \sin\gamma + 2\epsilon_0\epsilon_{31}g_{ij33}P_S \sin\gamma \end{aligned} \tag{19}$$

with $ij = 11, 22, 33$ and $13 = 31$.

In order to estimate the polarization-optic coefficients g_{ij11} given in (16) from the measured coefficients r_{ij1} we make some simplifying assumptions. We consider the spontaneous polarization to be directed exactly along the x-direction ($\gamma = 0$) and we assume that the polarization induced by the applied electric field $\mathbf{P}_{ind}$ also has only an x-component, that is we neglect the influence of the component ϵ_{31} of the dielectric tensor. Eqs. (19) then reduces to

$$r_{ij1} = 2\epsilon_0(\epsilon_{11} - 1)g_{ij11}P_S. \tag{20}$$

From (20) with $P_S \cong 14\ \mu C/cm^2$ and $\epsilon_{11} \cong 230$ one can estimate the quadratic polarization-optic coefficients

$$\begin{aligned} &g_{1111} \cong 0.31\ m^4/C^2, \quad g_{2211} \cong 0.16\ m^4/C^2, \\ &g_{3311} \cong 0.25\ m^4/C^2, \quad g_{1311} \cong -0.044\ m^4/C^2. \end{aligned} \tag{21}$$

These values agree relatively well with the results of crystal-optic measurements of [5] shown in (16). The values are higher than the ones from [5], indicating that the contribution of the second to fourth term in (19) has the same sign as those appearing in (21). As a consequence the coefficients g_{ii13} are suggested to be positive because ϵ_{31} is positive.

7. Conclusions

Free and clamped EO coefficients of $Sn_2P_2S_6$ for an electric field parallel to the crystallographic x-axis were determined with a direct interferometric technique for various wavelengths and temperatures. Both low-frequency EO measurements in a stress-free sample and measurements in the inertia-clamped samples using a step-like electric field were performed. The room temperature free EO coefficient r^T_{111} reaches 174 ± 10 pm/V at $\lambda = 633$ nm and shows only weak dispersion in the near infrared. It increases with temperature up to the ferroelectric to paraelectric phase transition at 65 °C, where a peak value of $r^T_{111} \cong 4500 \pm 110$ pm/V has been measured. The large values of r^T_{111} and r^T_{331} make of $Sn_2P_2S_6$ a very promising material for EO and photorefractive applications.

Acknowledgements

We are very grateful to the Swiss National Foundation for supporting this work (NF 20-66761.01 and SCOPES 7UKPJ062149).

References

[1] A. Anema, A. Grabar, T. Rasing, Ferroelectrics 183 (1–4) (1996) 181.
[2] M.I. Gurzan, A.P. Buturlakin, V.S. Gerasimenko, N.F. Korde, V.Y. Slivka, Sov. Phys. Solid State 19 (10) (1977) 1794 (Translated from Fizika-Tverdogo-Tela. 19 (10) (1977) 3068).
[3] S.G. Odoulov, A.N. Shumelyuk, U. Hellwig, R.A. Rupp, A.A. Grabar, I.M. Stoyka, J. Opt. Soc. Am. B (Opt. Phys.) 13 (10) (1996) 2352.
[4] A.A. Grabar, I.V. Kedyk, M.I. Gurzan, I.M. Stoika, A.A. Molnar, Y.M. Vysochanskii, Opt. Commun. 188 (1–4) (2001) 187.
[5] A.A. Grabar, Y.M. Vysochanskii, S.I. Perechinskii, L.A. Salo, M.I. Gurzan, V.Y. Slivka, Sov. Phys. Solid State 26 (11) (1984) 2087 (Translated from Fizika-Tverdogo-Tela. 26 (11) (1984) 3469.
[6] J. Kroupa, Y.I. Tyagur, A.A. Grabar, Y.M. Vysochanskii, Ferroelectrics 223 (1–4) (1999) 421.
[7] U. Hellwig, T. Leidlo, A.A. Grabar, I.M. Stoyka, R.A. Rupp, A.N. Shulmelyuk, S.G. Odoulov, in: Proceedings of Topical Meeting on Photorefractive Materials Effects and Devices, OSA Technical Digest Series, Chiba, Japan, 1997.
[8] A. Shumelyuk, S. Odoulov, D. Kip, E. Kratizig, Appl. Phys. B (Lasers and Optics) B 72 (6) (2001) 707.
[9] M. Weber, G. von Bally, A. Shumelyuk, S. Odoulov, Appl. Phys. B (Lasers and Optics) B 74 (1) (2002) 29.
[10] M. Sigelle, R. Hierle, J. Appl. Phys. 52 (6) (1981) 4199.

[11] C. Bosshard, K. Sutter, R. Schlesser, P. Gunter, J. Opt. Soc. Am. B (Opt. Phys.) 10 (5) (1993) 867.
[12] M. Aillerie, N. Theofanous, M.D. Fontana, Appl. Phys. B (Lasers and Optics) B 70 (3) (2000) 317.
[13] R. Spreiter, C. Bosshard, F. Pan, P. Gunter, Opt. Lett. 22 (8) (1997) 564.
[14] C.D. Carpentier, R. Nitsche, Mater. Res. Bull. 9 (4) (1974) 401.
[15] G. Dittmar, H. Schafer, Z. Naturforsch. 29B (5–6) (1974) 312.
[16] Y.M. Vysochanskii, M.I. Gurzan, M.M. Maior, E.D. Rogach, F.I. Savenko, V.Y. Slivka, Sov. Phys. Crystallogr. 35 (3) (1990) 459 (Translated from Kristallografiya 35 (3) (1990) 784.
[17] S.L. Bravina, L.S. Kremenchugskii, M.D. Kladkevich, N.V. Morozovskii, V.B. Samoilov, M.M. Maior, M.I. Gurzan, Y.M. Vysochanskii, V.Y. Slivka, Inorg. Mater. 23 (5) (1987) 657.
[18] I.S. Board, in: IEEE Standard on Piezoelectricity, IEEE, New York, 1987, p. 242.
[19] Y.M. Vysochanskii, V.Y. Slivka, Ferroelectrics of the $Sn_2P_2S_6$ Properties in Vicinity of Lifshitz Point, Oriana-Nova, 1994, p. 264 (in Russian).
[20] S.H. Wemple, M. DiDomenico Jr., in: R. Wolfe (Ed.), Electrooptical and Nonlinear Optical Properties of Crystals, vol. 3, Academic Press, New York, 1972, p. 264.
[21] M. DiDomenico Jr., S.H. Wemple, J. Appl. Phys. 40 (2) (1969) 720.
[22] R. Nitsche, P. Wild, Mater. Res. Bull. 5 (6) (1970) 419.
[23] A.A. Grabar, J. Phys.: Condens. Matter 10 (10) (1998) 2339.
[24] P. Gunter, M. Zgonik, Opt. Lett. 16 (23) (1991) 1826.
[25] F.P. Strohkendl, J.M.C. Jonathan, R.W. Hellwarth, Opt. Lett. 11 (5) (1986) 312.
[26] G.C. Valley, J. Appl. Phys. 59 (10) (1986) 3363.
[27] U. van Stevendaal, K. Buse, H. Malz, H. Veenhuis, E. Kratzig, J. Opt. Soc. Am. B (Opt. Phys.) 15 (12) (1998) 2868.
[28] P. Gunter, Opt. Commun. 11 (3) (1974) 285.